CuO and Ce-doped CuO Prepared by Microwave Hidrotermal Method in Photodegradation of Remazol Golden Yellow Dye

Max Rocha Quirino[a], Guilherme Leocárdio Lucena[a]* , Renata Júlia Cordeiro de Araújo[a],

Adriano Ribeiro da Silva[a], Anely Maciel de Melo[a], Ieda Maria Garcia dos Santos[b], Luciana Gama[c]

[a]*Universidade Federal da Paraíba, LABQUIM, Campus III, 58200-000, Bananeiras, PB, Brasil.*
[b]*Universidade Federal da Paraíba, NPE/LACOM, Campus I, 58059-900, João Pessoa, PB, Brasil.*
[c]*Universidade Federal de Campina Grande, UAEMa, Campus I, 58429-900, Campina Grande, PB, Brasil.*

Copper oxide (CuO) is a heterogeneous catalyst applied with success in several systems like vegetable oils transesterifications. The Ce-dopoing CuO is a promisor material with a potential improve catalysis performances. In this work, CuO and Ce-doping CuO were synthesized by the microwave hydrothermal method in only 5 min at low temperature (100 ºC) without templates or other petroleum dependent organic substances, using only copper and cerium nitrates and sodium hydroxide as a precursors. Both materials were applied as photocatalysts for the degradation of remazol golden yellow dye (RNL). X-ray diffraction analysis showed that CuO and Ce-doped CuO has monoclic copper oxide structure without secondary phases. SEM analysis showed the Ce-doping full modify the CuO powder morphology. The dye RNL degradation rate of Ce-doping CuO was bigger than pure CuO and the expensive CeO_2.

Keywords: *Ceramics, Catalytic proprieties, Chemical reaction, Nanostructures.*

1. Introduction

Copper oxide (CuO), narrow p-type semiconductor band gap, has been gaining much attention in the applied science and technology in the form of heterogeneous materials and because it particular properties[1-3]. This material is a metal transition oxide with optical properties to circulatory polarized light[4], photocatalytic activity[5], heterogeneous catalyst in the tranesterification of rubber oil (biodiesel)[6], sensors for volatile organic compounds[7], anode materials for Li ion battery[8], p–n homojunction to solar cells[9]. The Ce-doping CuO is interesting alternative to the expensive price of pure cerium oxide. Copper ceria catalysts is a kind of the most research catalytic system, which perfectly balanced the cost and the catalytic performance[10]. And Ce doped CuO systems shows improvement in the catalytic performances of this materials. Sing et al.[7] synthesized CuO hollow nanostructures that exhibit response for sensing acetone and as a resulting of doping with cerium, the material starts showing selectivity, highest response toward methanol sensing, and increasing the amount the Ce doping, the material shows high response for methanol and acetone. Guo et al.[10] synthesized $Cu_xCe_{1-x}O_2$ nanorods catalysts with a significant effect in CO-PROX reaction. Its observed that the Ce dopant cause a reduction of the band gap and shows a strong saturation magnetization, showing that this doped metal transition is a well diluted-magnetic semiconductor material[11]. CuO single phase material usually do not possess this better properties.

Is notorious the influence of Ce doped CuO. However, the synthesis usually applied long time, high temperatures and use petroleum precursors derived (templates). Chuai et al.[11] synthesized Ce doped CuO by the gas-liquid phase chemical deposition method at 820 ºC for 120 min to obtain the material phase. Jan et al.[12] obtained this material via chemical co-precipitation route. After preliminary process, the dried samples were annealed in electric furnace at 300 ºC for 2 h. Xing et al.[13] also synthesized via co-precipitation and the powders were calcined in a muffle furnace at 350 ºC for 3 h. Chen et al.[5] obtained Ce doped CuO nanostructures at low temperature (110 ºC) by the conventional hydrothermal method; they used cationic surfactant cetyltrimehyl ammonium (CTAB) and spend 6 h only in the synthesis. Guo et al.[10] realized a long time experiment (24 h) for the Ce doped CuO synthesis by the co-precipitation method at 500 ºC. Ponnar et al.[3] obtained this doped material by the microwave irradiation method in a domestic microwave oven and exposed to the microwave energy at short time (10 min) but the other steps like annealed the temperature for phase synthesis was 400 ºC during 3 h to guarantee the good crystallinity. Singh et al.[7] got Ce doped CuO hollow structures by the technique of inverse miniemulsion at 250 ºC for 4 h.

This is a promisor material (Ce doped CuO) for various applications. But this transition metal oxide is still little investigated and the synthesis for this catalytic system probably not obtained by the microwave hydrothermal method[14,15]. This method shows peculiar and unique characteristics like: direct dielectric heating in liquid and like a consequence, kinetics increased by 1 or 2 orders of magnitude, formation of new phases materials, low synthesis temperature, low cost with

*e-mail: guilhermelucena@cchsa.ufpb.br

electric energy, quickly reaching the working temperature saving energy / time and ecofriendly because reactions are carried out in closed systems[16-20].

Given the importance of improving ecofriendly techniques like the little studied MH method, especially in relation to Ce-doping CuO, the aim of this work was to synthesize, in mild conditions, single phase nanopowder of this material by the MH method without surfactants or templates and realize a catalyst performance for the photodegradation of Remazol Golden Yellow dye (RNL).

2. Materials and Methods

2.1. Materials

Cu(NO$_3$)$_2$.3H$_2$O (98% PROQUIMS), Ce(NO$_3$)$_3$·6H$_2$O (99% ALDRICH) and NaOH (99% PROQUIMS) were used for the synthesis of CuO, and Ce doped CuO nanoparticles discussed in this article. The distilled water was used as solvent. CeO$_2$ (99.9%) applied in the catalyst test was purchase from Aldrich.

2.2. Synthesis of CuO and Ce-doped CuO nanoparticles

Synthesis of the cooper oxide powder was synthesized by microwave hydrothermal method, as described in previous work[21]. Copper oxide was synthesized from a 90 mL solution (9x10^{-3} mol L^{-1}) of Cu(NO$_3$)$_2$, with addition of 8 mL solution (5 mol L^{-1}) of the mineralizing agent (NaOH). The solutions mixture was transferred to a Teflon and hydrothermalized autoclave at 100 °C for 5 minutes in a microwave hydrothermal reactor, INOVTEC, model RMW 1, using a frequency of 2.45 Hz and a power of 900 W, obtaining a black precipitate. The sample was wash with distilled water until pH = 7 and then, dried out at 110 °C for 12 h in oven.

For the Ce-doped CuO synthesis, 90 mL of a solution of Cu(NO$_3$)$_2$.3H$_2$O (M = 9x10^{-3} mol L^{-1}) were added 10 mL of Ce(NO$_3$)$_3$.6H$_2$O (M= 9x10^{-3} mol L^{-1}) solution . Same concentrations for both solutions varying the volume amount. And then was added 8 mL of NaOH (5 mol L^{-1}) solution resulting in a ratio of 1:9 (Ce:Cu) moles. The mixture was transferred to a Teflon autoclave and hydrothermalized at 100 °C for 5 minutes, obtaining a gray precipitate. Washing and drying of the material was performed same way as described above.

The CuO and Ce-doped CuO samples synthesized in this work were labeled CuNa05 and CeCuNa05, respectively.

2.3. Characterization

The structural nature of the synthesized CuNa05 and CeCuNa05 samples were detailed by powder x-ray diffraction method (XRD) using a Shimadzu XRD-6000 x-ray diffractometer with CuKα radiation (λ = 1.5406 Å) in the 2θ range of 10° to 80°, with a step size of 0.02° and step time of 2 s, at room temperature. The lattice parameters were calculated using the least square refinement from Rede 93 developed at UNESP (Araraquara, SP, Brazil). The volume of unit cell (V), average crystallite size (D), micro-strain (ε), dislocation density (S) and stacking fault (SF) were calculated using the equations 1 to 5, respectively[3].

$$V = a.b.c \, \sin \beta \tag{1}$$

$$D = \frac{0.9\lambda}{\beta cos\theta} \tag{2}$$

$$\varepsilon = \left(\beta.\cos\theta \right) / 4 \tag{3}$$

$$S = \frac{1}{D^2} \tag{4}$$

$$SF = \left[\frac{2\pi^2}{45\left(3\tan\theta\right)^{1/2}} \right].\beta \tag{5}$$

the parameters a, b and c are lattice constants, β denotes full width at half maximum (FWHM) of the highest intensity peak, θ is diffraction angle, λ is the wavelength of incident X-ray beam and π equal to 3.14.

The synthesized samples band gap were calculated from the UV-Vis spectra obtained in a Shimadzu model UV-2550 spectrophotometer, operating in reflectance mode, in the region of 190-900 nm. From the graphs of diffuse reflectance according to the method proposed by Tauc[22]. For this, it was used the Kubelka-Munk function mathematically described by Equation 6.

$$\left(h\nu\alpha \right)^{1/n} = A\left(h\nu - Eg \right) \tag{6}$$

Where: h is Planck's constant; ν is vibration frequency; α is absorption coefficient; A is the proportionality constant and Eg is the band gap energy. The exponent n values denote nature of samples transition. In this work, the n value that best fitted the data was ½, which corresponds to indirect transitions.

To identify the functional groups and to confirm the substitution of Ce ions, the samples were scrutinized with Fourier Transform Infrared Spectrometer using a Shimadzu IR-Prestige-21 spectrometer. The measurements were performed in the region between 400 and 2000 cm^{-1} using KBr as the beam splitter.

The morphology of the samples was studied via Scanning Electron Microscopy (SEM) using a Tescan Vega 3 microscope (Kohoutovice, Czech Republic). The samples were fixed on supports using copper tape and metallized with a thin layer of gold (Balzers Union, model FL 9496). The SEM micrographs were obtained with potential acceleration of 15 kV under low vacuum.

2.4. Photocatalytic and adsorption tests

The CuNa05, CeCuNa05 and commercial CeO$_2$ samples were used as photocatalysts for the degradation of RNL (molecular formula: C$_{16}$H$_{16}$N$_4$O$_{10}$S$_3$Na, weight: 546.99 g mol^{-1}, DyStar). The photocatalytic tests were performed in a homemade reactor with dimensions of 10 x 20 x 100 cm using UVC lamp (λ = 254 nm, 20 W, ILUMISAMPA). The experiments were carried out in triplicate using 10 mg of the photocatalyst and 10 mL of the dye solution with a concentration of 10 mg.L^{-1} at pH = 6. Petri dishes containing the dye solution and the photocatalysts were

photoirradiated for 1 h. After photocatalysis, the mixtures were centrifuged and filtered. The rate of discoloration and degradation of the dye solutions were quantified using a UV-vis spectrophotometer (Model UV-5100, Shimadzu) in absorbance mode. The photocatalytic efficiencies of the photocatalysts were calculated by calibration curves; the initial absorption of the untreated dye solution and the respective concentrations before and after photocatalytic treatment were considered. The rate of degradation is expressed by 7.

$$\text{Degradation rate} = \frac{(A_0 - A_t)}{A_0} \; x100\% \qquad (7)$$

where A_t and A_0 are absorbances at time t and zero, respectively.

In addition, tests were performed in the dark, using the same photocatalysis conditions tests, to evaluated only the solution discoloration in relationship adsorption of dye on the material surface.

3. Results and Discussion

3.1. Structural analysis

Figure 1 shows XRD patterns of the CuNa05 and CeCuNa05 samples synthesized by MH in 5 min, at 100 °C.

The XRD patterns show the characteristic peaks of monoclinic CuO (JCDPS card. n° 45-0937), The presence of secondary phases and/or impurities is not observed. At the *in set* of X-ray patterns, it clearly verified and confirm that are monophasic samples. The two most intense peaks are in 2θ = 35.58° and 38.86 associated to (002) e (111) planes, respectively. The synthesis using the MH method was efficient to obtain these materials in short time (5 mim) and low temperature (100 °C).

For CeCuNa05 sample, it was verified that the doping with cerium did not change the X-ray pattern, keeping the same profile of the CuNa05 sample, with only decrease in the intensity of the peaks were observed. When expanding the spectrum region between 34°-40° (*inset* Figure 1) it was certified that the dopant addition promoted a small shift (to the left) of the two most intense peaks of CuO. The peaks associated with the (002) and (111) planes were observed in

2θ = 35.44° and 38.67°, respectively. It was also observed that the difference of intensity between the both peaks was reduced with the addition of the dopant.

Singh et al.[7] showed that Ce-doped CuO synthesized by the microwave irradiation method, not the microwave hydrothermal (MH) method, revealed changes only in an intensity of X-ray patterns and attributed this diffractogram peaks modification confirms the presence of Ce into the CuO lattice. This observation becomes even more evident as the dopant concentration increases. However, no changes was found in the crystalline structures of the synthesized materials. That phases non-segregation of this materials, reforce, the obtaining of CuO doped with Ce.

Another investigation showed the synthesis of Ce doped CuO by hydrothermal conventional process (HC) at 100 °C for long time (6 h). It was observed formation of trace amounts of Cu_2O and the amount of this oxide are gradually strong with the increase dopant amount[5]. By the microwave hydrothermal process (MH) we synthesized only in 5 min at 100 °C without another phases . We note that MH process is efficient to obtain this single phase Ce doped CuO. Only shift toward lower Bragg angle (*inset* Figure 1), which that Ce ion were in to the CuO lattice successfully.

The lattice parameters (*a*, *b* e *c*), volume of the unit cell (V), average crystallite size (D), micro strain (ε), dislocation density (S) and stacking fault (SF) were calculated and displayed at Table 1.

According to the values showed in Table 1, the CuO (CuNa05) synthesized in this work presented the lattice parameters compatible with standard (JCPDS chart n° 45-0937), with a slight increase in the parameter *a* and in the angle β, and a small decrease in parameter *b*.

In relation to the CeCuNa05 sample, the dopant addition promoted a decrease in parameters *a* and in the β angle, besides to an increase in the values of parameters *b* and *c*. This alteration is associated with the difficulty of accommodation of Ce ions in the CuO lattice, since the ionic radius of Ce^{4+} (1.03 Å) and Ce^{3+} (0.93 Å) are greater than the ionic radius of Cu^{2+} (0.73 Å), the which leads changes at the network parameters. Similar results were observed in previous works reported in the literature[3,23,24].
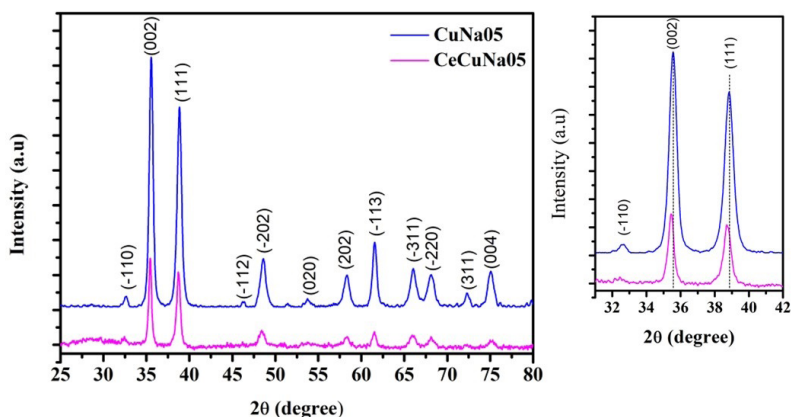
Figure 1. XRD patterns of the CuNa05 and CeCuNa05.

Table 1. Structural parameter of CuNa05 and CeCuNa05 nanoparticle.

Samples	Lattice constant			β (°)	V (Å)³	D (nm)	(ε)	S (x10⁻³)	SF
	a(Å)	b(Å)	c(Å)						
CuO*	4.69	3.43	5.13	99.55	81.4	-	-	-	-
CuNa05	4.71	3.41	5.13	99.93	81.2	16.50	0.3539	3.67	1.56
CeCuNa05	4.30	3.74	5.46	96.33	87.3	23.99	0.3534	1.74	1.50

* JCPDS card n. 45-0937

The crystallite size (D) of the CeCuNa05 sample when paralleled to CuNa05 was larger at 7.49 nm. This increase with the introduction of Ce is due to the amalgamation of particles, it is a result of solid state diffusion[3].

The results of micro-strain (ε), dislocation density (S) and stacking fault (SF) of CeCuNa05 showed a small decrease when pararelled to the undoped material (CuNa05). Similar results were observed by Ponnar et al.[3] when doping CuO with cerium.

It should be noted that SF corresponds to crystallographic disorganization and is considered a planar defect[25]. These defects are generated during the synthesis process and these modifications indicate that the formation of vacancies and/or defects were generated in to Cu-Ce-O lattice due to the dopant introduction. ε, S and SF decrements confirms the defects and vacancies are deduced by Ce doping. By the XRD analysis, it is possible to confirm that Ce is substituted in cupper oxide (CuO).

In Figure 2 the UV-Vis spectra of the CuNaO5 curves are observed with values of the energy extrapolation to determine the band gap energy spectra.

The monoclinic CuO theoretical band gap is order of 1.2 eV[26]. The band gap data obtained for the CuNa05 and CeCuNa05 samples 1.98 eV and 1.36 eV[26], respectively. In the CeCuNa05 sample, the band gap decrease, when compared to undoped sample, is associated with the symmetry break promoted by doping, which can be attributed to oxygen vacancies, network defects, impurities or distortions in chemical bonds, which promote the formation of localized energy levels within the materials gap.

Figure 3 shows the FT-IR spectrum of CuNa05 and CeCuNa05. The three characteristic peaks observed in the region of 400 - 600 cm⁻¹ are from the monoclinic CuO[27]. The peaks located between 421-430 cm⁻¹, 497-501 cm⁻¹ and 609 cm⁻¹ are attributed to the Cu-O bond stretching along the (-202), (101) and (202) directions, respectively[28-30]. The small width of these peaks indicate a high order at short range. Between 843-852 cm⁻¹, Cu-O-Cu lattice vibrations peaks are observed[3]. The samples presented bands at 1657 cm⁻¹ assigned to adsorbed H_2O and at 1042-1044 cm⁻¹ assigned to OH groups[31]. Band at 1384 cm⁻¹ is due to the atmospheric CO_2 absorption[32]. In relation ship CeCuNa05 sample, a small band observed at 932 cm⁻¹ refers to the stretching of the Ce-O metal-oxygen bond, thus confirms the presence of Ce into the CuO lattice. Ponnar et al.[3] when evaluating the FT-IR spectrum of Cu1-xCexO (x = 0; 0.02; 0.03; 0.05 and 0.07) verified band intensity of this spectrum region, increased in intensity as the amount of Ce in the lattice.

SEM micrographs of synthesized nanopowders of CuNa05 and CeCuNa05 are shown in Figure 4.

The copper oxide (CuNaO5) sample showed morphology like thin agglomerates lamellae. These clustered with sharp dendritic tendency smaller than 5 μm as shown
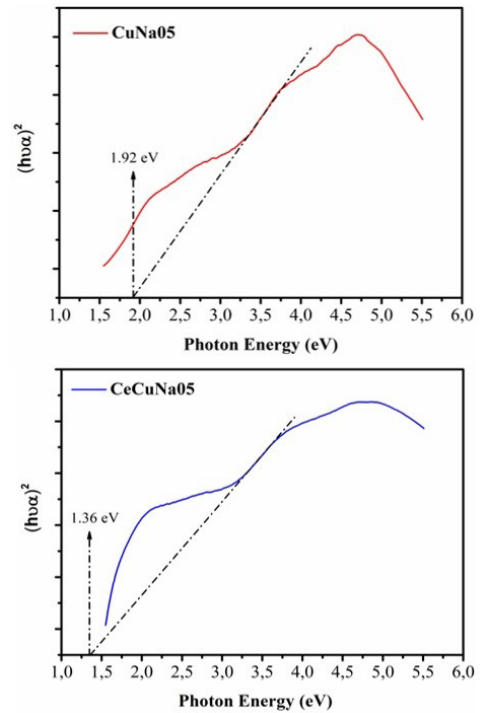
Figure 2. UV-vis spectrum of the CuNa05 and CeCuNa05.
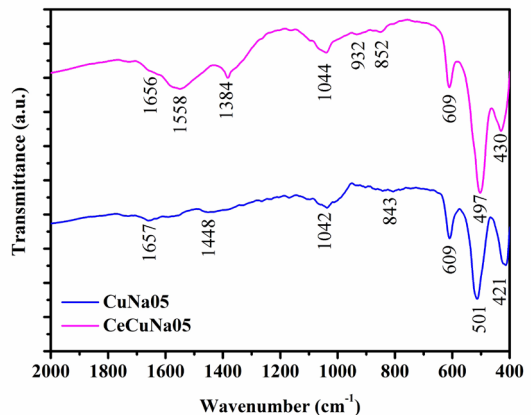
Figure 3. FT-IR spectrum of the synthesized CuNa05 and CeCuNa05.

in (Figure 4A and 4B). The sample doped with cerium (CeCuNa05) mophology was totally different from pure CuO (CuNa05). It is possible to observe large agglomerations with more rounded edges with irregular and rough surfaces
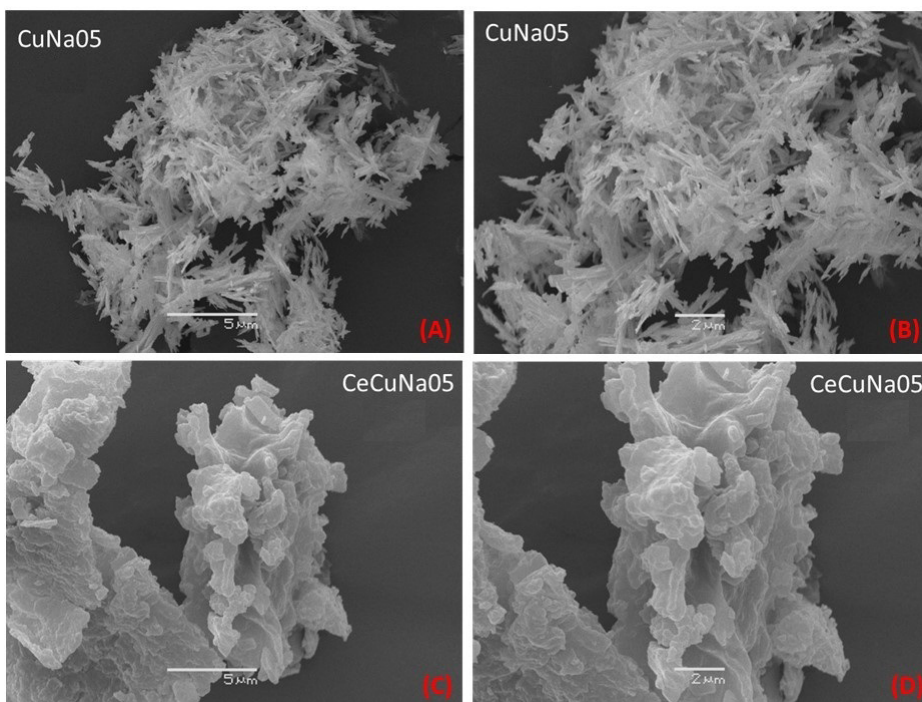
Figure 4. SEM micrographs of (A and B) CuNa05 and (C and D) CeCuNa05 samples.

(Fig 4C and 4D). These particles clusters smaller than 5 μm over clusters larger than 5 μm. The higher growth rate of the Ce-doped sample and its consequent change in morphology in comparison to the pure CuO sample is due to the Pauling electronegativity of Cu (1.9) being higher than that of Ce (1.1)[33,34]. The reactivity of the chemical element increases with decreasing Pauling electronegativity.

Zagaynov et al.[35] synthesized Ce doped CuO by sol-gel without secondary phases, using ethanol, dimethylloctyamine (DMOA). The xerogeels were calcinated at 500 °C for 4 h.

By the MH method it was observed that Ce doping totally influenced the morphology of the material, since the other synthesis parameters and route (reactants) were maintained.

3.2. Photocatalytic and adsorption evaluation

The UV-vis spectra and the discoloration percentages of the dye solution after adsorption and photocatalytic tests are displayed in Figures 5 and 6, respectively. It can be highlighted that RNL dye has a absorption in the vicinity of the wavelength 411 nm. This band is related to the azo bond[36].

For the adsorption tests, as the measurements were made in the dark environment, the decrease of the 411 nm band intensity was exclusively attributed to the reduction in the amount of dye in the solution due the adsorption on the surface of the material. For the solution treated with CeCuNa05, there was a very small adsorption (3%), while the other solution with CuNa05 reached a higher value (9%). These results can be understood considering the Coulomb forces of attraction and repulsion between the azo dye and the semiconductors.

As presented in Figure 6, UV irradiation had an important influence on the dye discoloration, which indicated that a photocatalytic reaction occurred. After 1 h
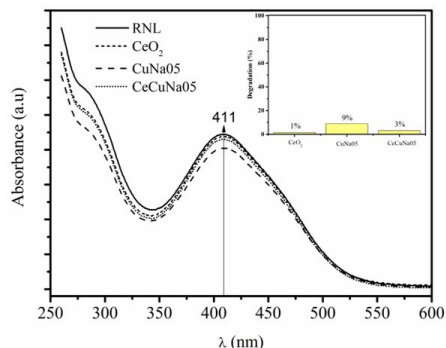
Figure 5. UV–vis spectra of an RNL solution after adsorption/1h test with CuNa05 and CeCuNa05.
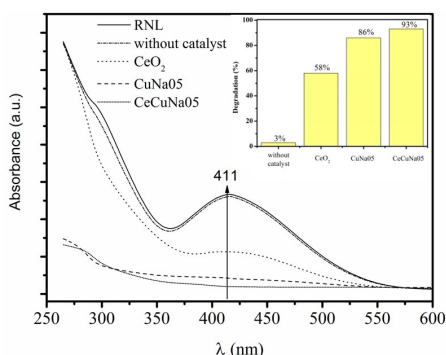
Figure 6. UV–vis spectra of an RNL solution after photocatalytic/1h test with CeO_2, CuNa05 and CeCuNa05.

of UV irradiation in the presence of CuNa05, CeO_2 and CeCuNa05 was able to decrease the absorption band of the azo bond by 86.5%, 57.9% and 92.5%, respectively. Compared with CeO_2, the addition of 10 mol% Ce in CuO increased by 35% in the rate degradation of RNL by expensive commercial CeO_2.

According to Liqiang et al.[37], when a semiconductor particle is irradiated by the light of energy higher or equal to the band gap energy, an electron from the valence band (VB) is excited to the conduction band (CB) with simultaneous generation of a hole (h⁺) in the VB. The e_{cb}^- and h_{vb}^+ can recombine on the surface or in the bulk of the particle in a few nanoseconds, or can be separated under the built-in electric field to transfer to different positions on the surfaces to react with donor (D) or acceptor (A) species adsorbed on or close to the surfaces. These phenomena contribute to catalysis performance.

The introduction of a dopant metal with a different charge promotes the formation of materials with defects and/or vacancies.

As shown in the Kröger-Vink notation (equation 8), the cerium introduction into the CuO crystal lattice promotes the formation of oxygen vacancy ($V_O^{\cdot\cdot}$), which directly influences the semiconductor photocatalytic properties.

$$CeO_2 \xrightarrow{CuO} Ce_{Cu}^{''} + 2O_O^X + V_O^{\cdot\cdot} \tag{8}$$
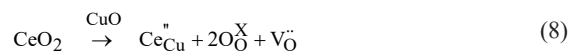
These vacancies can act as active centers for catalytic reaction, because the oxygen molecules of the defective oxides are likely to be easily released and transferred, which can increase the catalyst reactivity. Oxygen vacancies can promote O_2 adsorbing, and there is a strong interaction between the photo-induced electrons bound by oxygen vacancies and the adsorbed O_2[38].

Sasikala et al.[39] when evaluate the photodegradation of trypan blue and methyl orange dyes in presence of CuO doped with cerium catalistys, found that samples containing Ce^{3+} showed a higher concentration of oxygen vacancies and this favored a significant increase in photocatalytic activity. Similar results were observed by Ekthammathat et al.[40] in the photodegradation of methylene blue. The authors proposed that the Ce^{3+} incorporated into the CuO lattice was oxidized by releasing electrons to adsorbed O_2 to produce •O_2^- superoxide radicals with the subsequent formation of Ce^{4+}. And Ce^{4+} is reduced to Ce^{3+} by the absorption of photoexcited electrons from the CB of CuO as shown in equations 9 and 10.

$$Ce^{3+} + O_2 \rightarrow Ce^{4+} + \bullet O_2^- \tag{9}$$

$$Ce^{4+} + e^- \rightarrow Ce^{3+} \tag{10}$$

Islam et al.[41] reported that the doping of CuO with Ce, obtained by the sol-gel auto-combustion method, may be due to the increase in the mean lifetime of the electron and, thereby retarding the charge carrier recombination. Therefore, it can be inferred that the presence of cationic cerium in the copper oxide crystal lattice promoted an increase in the photocatalysis of the RNL dye.

4. Conclusion

CuO and Ce-doped were synthesized at low temperature and short time (5 min) by the ecofriendly MH method. The XRD analysis revealed CuO and Ce doped CuO without perceptive second phases (like Cu_2O or CeO_2 segregation). The SEM reveals that the introduction Ce in CuO lattice promoted total different surface morphology. The fotocatalyst band gap change promoted an improvement of RNL dye degradation. Finally, it be concluded that the Ce doped CuO was effective and a promisor as a photocatalytic in application in water purification and environment benign i.e. ecofriendly.

5. References

1. Sibhatu AK, Weldegebrieal GK, Sagadevan S, Tran NN, Hessel V. Photocatalytic activity of CuO nanoparticles for organic and inorganic pollutants removal in wastewater remediation. Chemosphere. 2022;300:134623.

2. Ighado JO, Sagboye PA, Umenweke G, Ajala OJ, Omoarukhe FO, Adeyanju CA, et al. CuO nanoparticles (CuO NPs) for water treatment: A review of recent advances. Environ Nanotechnol Monit Manag. 2021;15:100433-44.

3. Ponnar M, Thangamani C, Monisha P, Gomathi SS, Pushpanathan K. Influence of Ce doping onCuO nanoparticles synthesized by microwave irradiation method. Appl Surf Sci. 2018;449:132-43.

4. Duan Y, Liu X, Han L, Asahina S, Xu D, Cao Y, et al. Optically active chiral CuO "Nanoflowers". J Am Chem Soc. 2014;136:7193-6.

5. Chen Y, Tan H, Wu X, Sun Q, Wang D, Wang Y. Effect of doping Ce ions on morphology and photocatalytic activity of CuO nanostructures. Cryst Res Technol. 2019;54:1900033-6.

6. Sahu G, Gupta NK, Kotha N, Saha S, Datta S, Chavan P, et al. A review on biodiesel production through heterogeneous catalysis route. Chem Bio Eng Rev. 2018;5(4):231-52.

7. Singh I, Dey S, Santra S, Landfester K, Muñoz-Espí R, Chandra A. Cerium-doped copper(II) oxide hollow nanostructures as efficient and tunable sensors for volatile organic compounds. ACS Omega. 2018;3:5029-37.

8. Gao XP, Bao JL, Pan GL, Zhu HY, Huang PY, Wu F, et al. Preparation and electrochemical performance of polycrystalline and single crystalline CuO nanorods as anode materials for Li ion battery. J Phys Chem B. 2004;108:5547-51.

9. Han K, Tao M. Electrochemically deposited p–n homojunction cuprous oxide solar cells. Sol Energy Mater Sol Cells. 2009;93:153-7.

10. Guo X, Qiu Z, Mao J, Zhou R. Shape-controlled $Cu_xCe_{1-x}O_2$ nanorods catalyst and the active components functioned in selective oxidation of CO in hydrogen-rich stream. J Power Sources. 2020;451:227757-66.

11. Chuai M, Zhao Q, Yang T, Luo Y, Zhang M. Synthesis and ferromagnetism study of Ce doped CuO dilute magnetic semiconductor. Mater Lett. 2015;161:205-7.

12. Jan T, Iqbal J, Mansoor Q, Ismail M, Naqvi MSH, Gul A, et al. Synthesis, physical properties and antibacterial activity of Ce doped CuO:a novel nanomaterial. J Phys D Appl Phys. 2014;47:355301.

13. Xing M, Sun Q, Zeng C, Wang H, Zhao D, Zhang N, et al. Modulating Cu^+ distribution on the surface of Ce doped CuO composite oxides for SO_2^- resistant NH_3 selective catalytic reduction of NO. RSC Advances. 2017;7:18830-7.

14. Yang G, Park S. Conventional and microwave hydrothermal synthesis and application of functional materials: A review. Mater. 2019;12:1177-94.

15. Meng L, Wang B, Ma M, Lin K. The progress of microwave-assisted hydrothermal method in the synthesis of functional nanomaterials. Mater Today Chem. 2016;1-2:63-83.

16. Komarneni S, D'Arrigo MC, Leonelli C, Pellacani GC, Katsuki H. Microwave-hydrothermal synthesis of nanophase ferrites. J Am Ceram Soc. 1998;81:3041-3.

17. Komarneni S, Rajha RK, Katsuki H. Microwave-hydrothermal processing of titanium dioxide. Mater Chem Phys. 1999;61:50-4.

18. Komarneni S, Katsuki H. Nanophase materials by a novel microwave hydrothermal process. Pure Appl Chem. 2002;74(9):1537-43.

19. Moura AP, Cavalcante LS, Sczancoski JC, Stroppa DG, Paris EC, Ramirez AJ, et al. Structure and growth mechanism of CuO plates obtained by microwave-hydrothermal without surfactants. Adv Powder Technol. 2010;21:197-202.

20. Zawadzki M. Pd and $ZnAl_2O_4$ nanoparticles prepared by microwave-solvothermal method as catalyst precursors. J Alloys Compd. 2007;439(1-2):312-20.

21. Quirino MR, Lucena GL, Medeiros JA, Santos IMG, Oliveira MJC. CuO Rapid synthesis with different morphologies by the microwave hydrothermal method. Mater Res. 2018;21(6):e20180227.

22. Tauc J. Optical Properties of Solids. Amsterdam : North-Holland, 1972.

23. Harish S, Navaneethan M, Archana J, Ponnusamy S, Muthamizhchelvan C, Hayakawa Y. Chemical synthesis and properties of spindle-like CuO nanostructures with porous nature. Mater Lett. 2015;139:59-62.

24. Bouazizi N, Bargougui R, Oueslati A, Benslama R. Effect of synthesis time on structural, optical and electrical properties of CuO nanoparticles synthesized by reflux condensation method. Adv Mater Lett. 2015;6(2):158-64.

25. Fine EM. Introduction to chemical and structural defects in crystalline solids. In: Hannay NB, ed. The chemical structure of solids. vol 1. New York: Springer; 1973. p. 288-333.

26. Wang L, Kang Y, Wang Y, Zhu B, Zhang S, Huang W, et al. CuO nanoparticle decorated ZnO nanorod sensor for low-temperature H_2S detection. Mater Sci Eng C. 2012;32:2079-85.

27. Xu Y, Chen D, Jiao X. Fabrication of CuO pricky microspheres with tunable size by a simple solution route. J Phys Chem B. 2005;109:13561-6.

28. Erdogen IY, Gullu O. Optical and structural properties of CuO nanofilm: its diode application. J Alloys Compd. 2010;492(1-2):378-83.

29. El-Trass A, Elshamy H, El-Mehasseb I, El-Kemary A. CuO nanoparticles: Synthesis, characterization, optical properties and interaction with amino acids. Appl Surf Sci. 2008;258(7):2997-3001.

30. Prathap MUA, Kaur B, Srivastava R. Hydrothermal synthesis of CuO micro-/nanostructures and their applications in the oxidative degradation of methylene blue and non-enzymatic sensing of glucose/H_2O_2. J Colloid Interface Sci. 2013;370(1):144-54.

31. Maul J, Brito AS, Oliveira ALM, Lima SJG, Maurera MAMA, Kelson D, et al. Influence of the synthesis media in the properties of CuO obtained by microwave-assisted hydrothermal method. J Therm Anal Calorim. 2011;106:319-23.

32. Zhao Y, Frost RL, Yang J, Martens WN. Size and morphology control of gallium oxide hydroxide GaO(OH), nano- to micro-sized particles by soft-chemistry route without surfactant. J Phys Chem C. 2008;112(10):3568-79.

33. Chen Y, Tan H, Wu X, Sun Q, Wang D, Wang Y. Effect of doping Ce ions on morphology and photocatalytic activity of CuO nanostructures. Cryst Res Technol. 2019;54:19000332.

34. Yang S, Hong S, Tsai C. Growth mechanisms and characteristics of ZnO nanostructures doped with In and Ga. Jpn J Appl Phys. 2010;49(6S), 06GJ06.

35. Zagaynov IV, Kutsev SV, Shelekhov EV, Naumkin AV. CuO–CeO_2 composites: synthesis from mixed sols. Colloids Surf A Physicochem Eng Asp. 2014;444:159-64.

36. Catanho M, Malpass GRP, Motheo AJ. Evaluation of electrochemical and photoelectrochemical methods for the degradation of three textile dyes. Quim Nova. 2006;29:983-9.

37. Liqiang J, Xiaojun S, Weimin C, Xiaoqian L, Honggang F, Haige H, et al. Photoluminescence of Ce doped TiO_2 nanoparticles and their photocatalytic activity. Acta Chimi Sin. 2003;61(8):1241-5.

38. Jing LQ, Zheng YG, Xu ZL, Dong FX, Sun XJ, Cai WM, et al. Electronic paramagnetic resonance characteristics of ZnO ultrafine particles and their photocatalytic performance. Chem J Chin Univ. 2001;22(11):1885-8.

39. Sasikala R, Karthikeyan K, Easwaramoorthy D, Bilial IM, Rani SK. Photocatalytic degradation of trypan blue and methyl orange azo dyes by cerium loaded CuO nanoparticles. Environ Nanotechnol Monit Manag. 2016;6:45-53.

40. Ekthammathat N, Phuruangrat A, Thongtem T, Thongtem S. Synthesis and characterization of Ce-doped CuO nanostructures and their photocatalytic activities. Mater Lett. 2016;167:266-9.

41. Islam MR, Saiduzzaman M, Nishat SS, Kabir A, Farhad SFU. Synthesis, characterization and visible light-responsive photocatalysis properties of Ce doped CuO nanoparticles: a combined experimental and DFT+U study. Colloids Surf A Physicochem Eng Asp. 2021;617:126386.